buildings

MDPI

Article

Optimizing the Design of Container House Walls Using Argon and Recycled Plastic Materials

Issa Omle [1], Ali Habeeb Askar [1,2,3] and Endre Kovács [1,*]

[1] Institute of Physics and Electrical Engineering, University of Miskolc, 3515 Miskolc, Hungary; issa.omle@uni-miskolc.hu (I.O.); 20156@uotechnology.edu.iq (A.H.A.)
[2] Department of Fluid and Heat Engineering, University of Miskolc, 3515 Miskolc, Hungary
[3] Mechanical Engineering Department, University of Technology—Iraq, Baghdad 10066, Iraq
* Correspondence: kendre01@gmail.com or endre.kovacs@uni-miskolc.hu

Abstract: Interest in the use of container houses has been increasing in recent years because of their resistance to earthquakes and fires. The incorporation of recyclable materials into these houses will simultaneously reduce energy use and greenhouse gas emission rates. In this context, the thermal performance of an external multi-layer wall of a container house mostly made of recyclable materials is studied and compared to that of a normal wall. The current study proposes a completely new structure, where there are air gaps and plastic layers between the steel sheets to enhance thermal insulation. In these gaps, different gases including argon are tested to reduce the heat loss. Calculations are carried out for a steady-state case in the winter season using the student version of ANSYS 2023 R2 Academic software, and the heat loss is calculated for different materials and different thicknesses of the wall layers. Afterward, based on a life-cycle cost analysis, the optimum air gap materials, optimum thickness of plastic and air gap, and energy savings are determined for a period of 20 years. We found that the optimum number of plastic layers to minimize the heating load is 21, but this reduces to 11 when considering economic factors. Furthermore, if a reflective layer covers the plastic layer, the optimum is just one layer. For an insulation thickness of 2 cm, the maximum total life-cycle savings are 335.14 and 350.52 USD, respectively, and the minimum ones are 16.06 and 31.44 USD, respectively, for multi-layer walls with and without reflective layers compared to conventional walls.

Keywords: argon insulation; container houses; recycled materials; radiation effect; optimization; FEM simulation

Citation: Omle, I.; Askar, A.H.; Kovács, E. Optimizing the Design of Container House Walls Using Argon and Recycled Plastic Materials. *Buildings* **2024**, *14*, 3944. https://doi.org/10.3390/buildings14123944

Academic Editor: Jiho Moon

Received: 4 November 2024
Revised: 30 November 2024
Accepted: 9 December 2024
Published: 11 December 2024

1. Introduction

The burgeoning interest in the application of recycled materials for thermal insulation in buildings has been a notable trend in recent years [1,2]. The integration of these materials into building envelopes has the potential to significantly reduce energy consumption, greenhouse gas (GHG) emissions, and environmental impact using recycled materials in building construction and envelope design [3].

It is known that from the point of view of conduction, the best insulator is a vacuum followed by some gases. The question immediately arises as to why we do not use them to insulate our buildings. The main reason is that heat can transfer easily through them by radiation and convection. The second reason is that to be contained, they need a vessel, which may be expensive. In the case of container houses, the vessel can be the metal wall itself if one considers not a single but a double wall with a sandwich structure or if a phase-change material (PCM) is integrated into the container [4]. On the other hand, radiative and convective heat transfer can be inhibited by thin intermittent layers.

The field of thermal insulation has been the subject of extensive research due to its significant implications for energy efficiency, cost-effectiveness, and environmental impact [5].

Studies by Luis E. [6], Mavromatidis Lazaros et al. [7], Dina S. Noaman et al. [8], and Hassan Kareem et al. [9] collectively explored the thermal efficiency and environmental implications of various multi-layer thermal insulation systems, including designs with multiple air chambers, expanded polystyrene (EPS) layers, medium-density fiberboard (MDF) panels, and optimal air gap thicknesses, highlighting their potential for material savings, enhanced thermal resistance, and energy-efficient construction.

D. Borelli et al. [10] defined a system to evaluate the optimal thickness of insulation for various climatic zones in relation to the yearly energy balance, considering both heating and cooling seasons; meanwhile, Nurlan Zhangabay et al. [11] developed air-gap energy-saving enclosing structures.

Additionally, Walla Naje et al. [12] analyzed the temperature distribution across room walls using Ansys Fluent with air gaps of 8 cm, 5 cm, and 2.5 cm; these studies collectively enhance our understanding of thermal insulation systems and their implications for energy efficiency, cost-effectiveness, and environmental impact, providing valuable insights into sustainable construction practices and energy-efficient design.

Numerous empirical studies estimate the ideal thickness of thermal insulation materials in building walls, accounting for factors such as climate, economic considerations (e.g., inflation, discount rate, longevity, and energy expenses), and building characteristics (e.g., heating/cooling loads, wall construction, and insulation material properties).

Life-cycle cost analysis-based economic models are often used to determine the optimal insulation thickness and payback time. These studies indicate that higher heating and cooling energy demands, longer building lifespans, inflation rates, energy prices, and insulation material thermal conductivity tend to increase the ideal insulation thickness. Conversely, higher discount rates, insulating material costs, total wall resistance, the coefficient of performance (COP) of cooling systems, and solar radiation incident on walls decrease the optimal thickness.

Furthermore, these characteristics significantly influence life-cycle costs, payback times, and energy savings [13].

Sadrzadehrafiei et al. [14] conducted a study in a tropical climate, specifically in Malaysia, to investigate the impact of triple glazing on cooling energy. The study examined the energy savings in cooling through the use of triple glazing compared to a single layer of transparent glass. Compared to single transparent glass, triple glazing reduced cooling electricity use by 6.3%, according to the study. Although the difference was not statistically significant, triple glazing with a 16 mm air gap resulted in higher savings than triple glazing with a 15 mm air gap.

Another investigation, conducted on a building in Tripoli, Libya, indicated that levels facing south greatly add to total energy consumption, with a rise in energy consumption of between 6 and 181% corresponding to an increase in the number of front windows [15]. Several researchers have pointed out that air conditioning systems account for a considerable portion of commercial buildings' overall yearly electricity consumption [16].

According to studies conducted in hot desert areas, a building's cooling demand is 45 percent attributable to its glass façade [17,18]. Baetens et al. [17,18] also conducted a literature assessment, exploring smart windows as a means to dynamically control solar energy and daylight in buildings. Transparent conductors and electrochromic windows made of various metal oxides and polymers were among the approaches covered in this research. Compared to blinds, these smart windows cut illumination energy use by about 26%, and in warmer climates such as California, USA, they can cut peak cooling loads by about 20%.

Hamidul Islam et al. [19] examined the use of shipping containers for buildings, focusing on their carbon footprint and life-cycle environmental impacts, concluding that these impacts increase significantly if the building's design life extends to 100 years.

Okan Kon and Ismail Caner [20] explored thermal insulation criteria for five temperature zones in Turkey's TS 825 standard, determining the minimum insulation thickness, life-cycle savings (LCS), life-cycle total cost (LCTC), energy savings (ES), and payback

period over ten years. They compared minimum and optimum insulation thicknesses for LCS and LCTC based on energy consumption and savings, using materials such as XPS, EPS, glass wool, rock wool, and polyurethane.

Maryam Dlimi et al. [21]. highlighted the growing popularity of bio-based thermal insulating materials, which reduce energy usage and GHG emissions [22].

A life-cycle cost study determined the optimal hemp wool thickness, energy savings, and payback time over 20 years. The 1D heat equation was solved using MATLAB for various wall orientations, finding maximum insulation thicknesses of 5 cm for east and west and 4 cm and 3 cm for south and north, respectively. Adding an air gap layer optimized insulation further, with a thickness of 1.3 cm for all orientations, cutting yearly GHG emissions by 71% [23].

Studies on multi-layer thermal insulation systems, including those with air chambers and various insulating materials, demonstrate significant material savings and enhanced thermal resistance. Optimal insulation thickness varies based on climatic zones, building characteristics, and economic factors, with life-cycle cost analysis playing a crucial role in determining the best solutions. The enhancement of Trombe wall systems' efficacy in specific climates by inert gases, particularly argon, is demonstrated. Both the experimental and numerical investigations evidenced the minimal effects of channel width and vent height variations. However, the air gap width and storage wall thickness were identified as critical components. Substituting argon for air in the air gap significantly enhances the system's efficiency by approximately 14.8%. Employing argon gas can enhance the cost-effectiveness and efficiency of passive heating systems in regions with comparable climates. Adding argon to Trombe wall systems results in enhanced overall performance and more consistent interior temperatures [23].

In our current work, we continue the above-mentioned investigations. Since, according to our best knowledge, nobody examined container houses where there is an air-gap or argon layer between two metal sheets up to now, there is a remarkable research gap here. We use Ansys Workbench solutions that help engineers solve the most complex thermal challenges and predict how their designs will perform with temperature changes. We use various solvers, including Minitab 2023 Version 21.4.1, Isight 2019 version 6.3, and the student version of ANSYS 2023 R2 Academic software, to systematically evaluate the optimal design. Therefore, the paper is organized as follows: Section 2 provides the definition of design steps and conditions for the simulation of the model's wall, including materials, equations, and boundary conditions, and Section 3 displays the verification. Section 4 displays the first round of simulation by Ansys and optimization by design tools. Section 5 presents the second round of simulation and optimization heat transfer results and the economic feasibility study, while Section 6 concludes with a summary of our results.

2. Design Steps

2.1. Geometry

A simulation model was developed to represent a section of a wall with different designs as can be seen in Figure 1. The dimensions in y and z are 1 m $\times$ 1 m, respectively. After the design has been completed, the models will be compared in terms of heating loads and economic feasibility.

The first type of design involves the use of conventional materials, such as brick and concrete, depicted by Figure 1A,B. Figure 1A shows three layers: an internal plaster layer, a brick layer, and an external cement layer. The wall in Figure 1B comprises four layers: an internal plaster layer, a concrete layer, an insulating layer (EPS and glass wool), and an external cement layer.

The second design is the proposed container house, which mostly involves the use of recycled or recyclable materials, such as steel and recycled plastic. Figure 1C illustrates the components of the proposed walls, whereas the optimal design tool aims to minimize heat and cost by matching the values of input parameters. To enhance aesthetics and comfort, we placed a layer of wood on the inside, which also helps to decrease heat loss. The steel

provides stability to the structure of the house against earthquakes [24] and reduces the risk of fires. Additionally, it acts as a container that contains the layers of gas, which are separated by panels made of recycled plastic. The walls of container houses are usually made of corrugated plates. For the sake of simplicity, we assume flat steel sheets instead. The layers of steel on the inside and outside are very good heat conductors. There may be places where the inner and outer steel layers touch each other (joints between parts of the house), which work as thermal bridges. To reduce their effect, we assume an insulation layer on the outside made of the same EPS as in the case of the conventional wall.

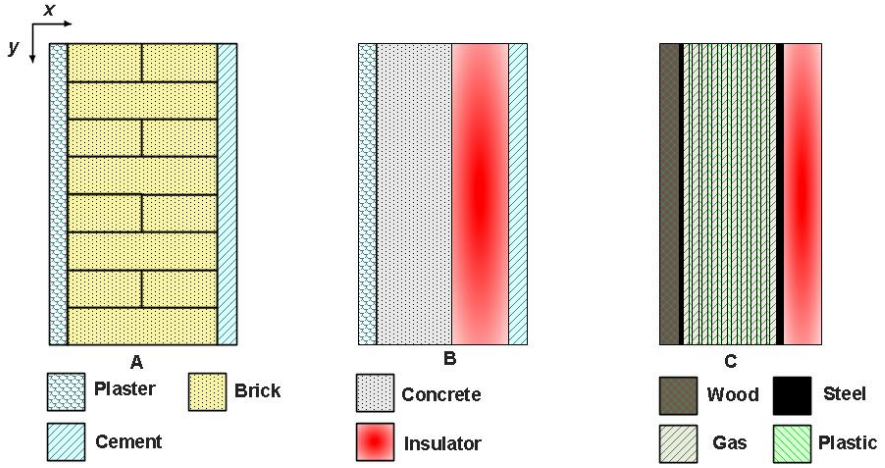

Figure 1. The components of the three walls. (**A**) Brick wall without insulation. (**B**) concrete wall with insulation. (**C**) the proposed wall of the container house.

In the calculations, the thickness of wall A without insulation is 0.27 m, whereas the thickness of plaster and cement is 0.01 m each, while the brick is 0.25 m. The thickness of wall B with EPS and glass-wool insulation is 0.265 m, where the thickness of the concrete is 0.12 m, that of the insulation is 0.125 m, and the thickness of the plaster and cement is the same as in wall A. In Section 5, for wall C, based on the optimal design, the total thickness of the wall is fixed at 154 mm with dimensions based on the optimization of the overall thickness of the wood layer at 10 mm, the thickness of the two layers of steel at 2 mm and 4 mm, and the EPS thickness at 20 mm. The thickness of the plastic panels is also fixed at 2 mm. We then vary the number of plastic layers in the gas (between the 0.118 fixed distance steel layers) to achieve the desired thickness.

2.2. Material Properties

The current study takes into account the real material properties listed in Table 1. Note that these coefficients are not affected by changes in temperature, time, or space because they are considered constants inside a material. We used a cement layer for external surfaces as it withstands harsh environmental conditions, and we used a gypsum plaster for internal surfaces because it offers a clean and aesthetic look to interiors.

Table 1. The properties of the materials used [25–27].

Materials	$\rho(\mathbf{kgm^{-3}})$	$c(\mathbf{Jkg^{-1}K^{-1}})$	$k(\mathbf{Wm^{-1}K^{-1}})$	Price ($/m^3)
Brick	1900	840	0.73	65
Concrete	2400	850	1.95	300
EPS insulation	320	1400	0.038	97.067
Glass-wool insulation	700	120	0.039	70
Gypsum plaster	1700	1000	0.726	50
Cement	2000	880	0.954	25
Wood	625	1300	0.12	694.25

Table 1. *Cont.*

Materials	$\rho(\mathbf{kgm^{-3}})$	$c(\mathbf{Jkg^{-1}K^{-1}})$	$k(\mathbf{Wm^{-1}K^{-1}})$	Price ($/m^3)
Steel	7800	840	60.5	5109
Argon	5.704	0.3122	0.0158	5
Air	1.225	1005	0.0242	2
CO_2	1.87	763	0.0166	50
Plastic	1250	880	0.15	800
Aluminum foil	2710	903	235	6330

2.3. Governing Equations and Solution Method

The approximations and hypotheses are the following:

1. Ansys Fluent is used to simulate convective, conductive, and radiative heat transfer within the cavities of the layers.
2. It is assumed that the cavities' inner walls are gray, diffuse, and opaque.
3. The cavities are filled with gas, and the Boussinesq buoyancy hypothesis is adopted.
4. The flow field is described as two-dimensional steady-state flow, i.e., $\partial u/\partial t = 0$, $\partial v/\partial t = 0$.

2.3.1. Governing Equations

The two-dimensional governing equations can be written as follows [28].

- The continuity equation (conservation of mass principle)

$$\frac{\partial u}{\partial x} + \frac{\partial v}{\partial y} = 0 \tag{1}$$

where u and v are the x- and y-component of the velocity (m/s), respectively.

- The momentum equations (conservation of momentum principle)
  - along the x-axis

$$\rho(u\frac{\partial u}{\partial x} + v\frac{\partial u}{\partial y}) = -\frac{\partial p}{\partial x} + \mu(\frac{\partial^2 u}{\partial x^2} + \frac{\partial^2 u}{\partial y^2}) \tag{2}$$

  - along the y-axis

$$\rho(u\frac{\partial v}{\partial x} + v\frac{\partial v}{\partial y}) = -\frac{\partial p}{\partial y} + \rho g\beta(T - T_\infty) + \mu(\frac{\partial^2 v}{\partial x^2} + \frac{\partial^2 v}{\partial y^2}) \tag{3}$$

where $\rho g\beta(T - T_\infty)$ is the buoyancy Boussinesq approximation, ρ is density (kg/m^3), β is the coefficient of thermal expansion (K^{-1}), μ is dynamic viscosity (kg/(ms)), g is the gravitational acceleration of the Earth (m/s^2), T is the temperature of the fluid (gas), and T_∞ is the temperature of the quiescent fluid away from the surface.

- The energy equation (conservation of energy principle)

$$\left(u\frac{\partial T}{\partial x} + v\frac{\partial T}{\partial y}\right) = \frac{k}{\rho c}\left(\frac{\partial^2 T}{\partial x^2} + \frac{\partial^2 T}{\partial y^2}\right) + q, \tag{4}$$

where k is thermal conductivity coefficient (W/(mK)) and c is specific heat (J/(kgK)), q is the heat source (W/m^3).

The governing equations of natural convection are often non-dimensional, and in order to reduce the total number of variables, the variables are combined to form non-dimensional numbers.

- Dimensionless numbers

The Prandtl number is physically defined as the ratio of the momentum diffusivity ν to the thermal diffusivity α. It provides a measurement of the effectiveness of diffusion transfer through the velocity and thermal boundary layers; it is given as follows:

$$Pr = \frac{\nu}{\alpha} \tag{5}$$

In terms of physics, Rayleigh number is the ratio of buoyancy, and the viscosity forces multiplied by the ratio of momentum and the thermal diffusivities. It is defined as follows:

$$Ra = \frac{g\beta\Delta TL^3}{\nu\alpha} \tag{6}$$

where L is the characteristic length (m), ΔT is the characteristic temperature difference (K), and ν is the kinematic viscosity coefficient (m^2/s). Most heat transfer below the crucial Rayleigh number is accounted for via conduction. Convection is largely responsible for heat transfer above this threshold temperature.

The ratio of convective to conductive heat transfer across the boundary is known as the Nusselt number. It can be defined as

$$Nu = \frac{Q_{conv}}{Q_{cond}} = \frac{[hA(T_1 - T_2)]}{\left[\frac{kA(T_1 - T_2)}{L}\right]} = \frac{hL}{k} \tag{7}$$

where h is the convective heat transfer coefficient of the flow ($W/(m^2K)$), A is the heat transfer surface area (m^2), T_1 is the temperature of the surface of the solid wall, and T_2 is the temperature of the fluid (gas) far from the surface. Consequently, the strength of convective heat transfer in relation to conduction heat transfer through the liquid is indicated by the Nusselt number. This indicates that as the Nusselt number rises, convective heat transfer becomes dominant.

- The results of the validation part were calculated in Fluent according to the following equations:

$$q_{tot} = \frac{1}{A}\int q_{local} \cdot dA = q_{rad} + q_{conv} \tag{8}$$

$$Nu_{conv} = \frac{q_{conv} \cdot L}{k(T_h - T_c)} \tag{9}$$

$$Nu_{rad} = \frac{q_{rad} \cdot L}{k(T_h - T_c)} \tag{10}$$

$$Nu_{tot} = \frac{1}{A}\int Nu_{local} \cdot dA = Nu_{rad} + Nu_{conv} \tag{11}$$

where T_h is the temperature of the hot surface, and T_c is the temperature of the cold surface.

2.3.2. The Equations' Discretization

In computational fluid dynamics (CFD), the conservation equations that govern the flow (the physical model) are written for each cell [29], and then the previous set of differential equations are converted into a set of algebraic equations according to what is called discretization, and then solving them using one of the methods used in numerical solution [30]. To achieve the coupling and correlation between velocity and pressure in the continuity and momentum equations, SIMPLE (Semi-infinite method for pursuer linked equation) is utilized. For the discretization of equations, a second-order interpolation is applied to the energy and momentum equations, as the mesh of the geometric model is smooth. The results are more accurate when using the second-order approximation compared to a rough mesh, where the second-order approximation may yield less accurate results, making a first-order approximation preferable (Ansys Fluent User Guide). For pres-

sure interpolation, the Body Force Weighted scheme is recommended for free convection modeling (Ansys Fluent User Guide) [31].

The results of the solution are typically displayed either as colored images describing the flow structure or as graphical curves that are analyzed to provide an approximate picture of the system's behavior. The final step involves verifying the validity of the solution by comparing these results with experimental data or with the findings of previous researchers. This is performed through logical approximations related to the numerical solution, such as monitoring the general convergence criterion and observing the value of a specific point or surface.

2.3.3. Radiative Heat Transfer Handling

Radiation exchange between diffuse gray surfaces within an enclosure may be accounted for using the surface-to-surface (S2S) radiation model. The energy exchange between two surfaces depends in part on their separation distance, size, and orientation. A geometric function known as a "view factor" is responsible for these features.

The S2S radiation model assumes that all surfaces are diffuse and gray. Thus, if a certain amount of radiation is incident on a surface according to the gray-body model, then a fraction is absorbed, a fraction is reflected, and a fraction is transmitted. The surfaces in question are opaque to thermal radiation (in the infrared spectrum) for most applications; therefore, the surfaces can be considered opaque.

The net rate of heat transfer by radiation between two surfaces i and j forming a closed space can be calculated using the following equation:

$$Q_{ij} = \frac{\sigma\left(T_i^4 - T_j^4\right)}{R_i + R_{ij} + R_j} = \frac{\sigma\left(T_i^4 - T_j^4\right)}{\frac{1-\varepsilon_i}{A_i\varepsilon_i} + \frac{1}{A_iF_{ij}} + \frac{1-\varepsilon_j}{A_j\varepsilon_j}} \tag{12}$$

where $\frac{1-\varepsilon_i}{A_i\varepsilon_i}$ and $\frac{1-\varepsilon_j}{A_j\varepsilon_j}$ are the radiation resistance of the surfaces; $\frac{1}{A_iF_{ij}}$ is the space resistance to radiation; ε is the radiation emissivity; and σ is the Stefan–Boltzmann constant, which is equal to $5.67 \cdot 10^{-8} \frac{\mathrm{W}}{\mathrm{m}^2 \cdot \mathrm{K}^4}$.

The view factor can be calculated using the following equation:

$$F_{ij} = F_{A_i \to A_j} = \frac{\dot{Q}_{A_i \to A_j}}{\dot{Q}_{A_i}} = \frac{1}{A_i} \iint\limits_{A_iA_j} \frac{cos\theta_i cos\theta_j}{\pi r^2} dA_i dA_j, \tag{13}$$

where i, j denote the surface number; dA_i and dA_j the cross-sectional area of the radiating and receiving surfaces, respectively; r is the distance between the surfaces dA_i, dA_j; and θ_i, θ_j are the angles between the normal of the two surfaces and the line connecting the surfaces, respectively.

In Ansys Fluent, when using the S2S radiation model, q in the energy equation can be replaced as follows:

$$q \sim Q_{rad} \cong Q_{ij} = \frac{\sigma\left(T_i^4 - T_j^4\right)}{R_i + R_{ij} + R_j} = \frac{\sigma\left(T_i^4 - T_j^4\right)}{\frac{1-\varepsilon_i}{A_i\varepsilon_i} + \frac{1}{A_iF_{ij}} + \frac{1-\varepsilon_j}{A_j\varepsilon_j}}, \tag{14}$$

2.3.4. The Equations Used for Economic Calculations Study

In the calculations, the following equations are used:

$$Q_{annual} = \frac{q \times time}{1000} = \frac{q \times 3 \text{ months } \times 30 \text{ days } \times 24 \text{ hours}}{1000}.$$

where Q_{annual} is the annual (winter) heat energy loss in [kWh/m^2], q is heat loss in [W/m^2].

$$LCPE = Q_{annual} \times \text{System lifetime } \times \text{cost of energy.}$$

where $LCPE$ is life-cycle price of energy in [USD], System lifetime [20 years], and the cost of energy is 0.12 [USD/kWh].

$$LCC = \text{ Total initial cost} + \text{Life cycle price of energy.}$$

where LCC is total life-cycle cost in [USD], total initial cost (initial investment) is the cost of all used materials.

We use this number LCC as the basis indicator for optimization since the final goal is to provide affordable housing with a comfortable temperature inside.

The simulation will be started by Fluent Flow. First, the geometry will be created by Design Modeler, and the next step will be meshing in the next section.

2.4. Mesh Construction

In this research, the studied domain is meshed using the Ansys meshing application program. Undoubtedly, adding more computational cells can yield a more accurate result, but we must remember that this will come at a higher computational expense [32]. The results remain consistent beyond a certain number of cells, indicating that mesh independence has been achieved. To verify the independence of the results on the mesh density, ten meshes with an increasing total number of elements for wall C with one plastic layer are used. We calculate the heat loss based on the number of elements. Figure 2 illustrates that the heat loss does not change when the number of elements is increased beyond 63,000. Accordingly, we fixed an element size of 0.0008 m, such that the cells were square cuboids, and the total number of elements was 63,000.

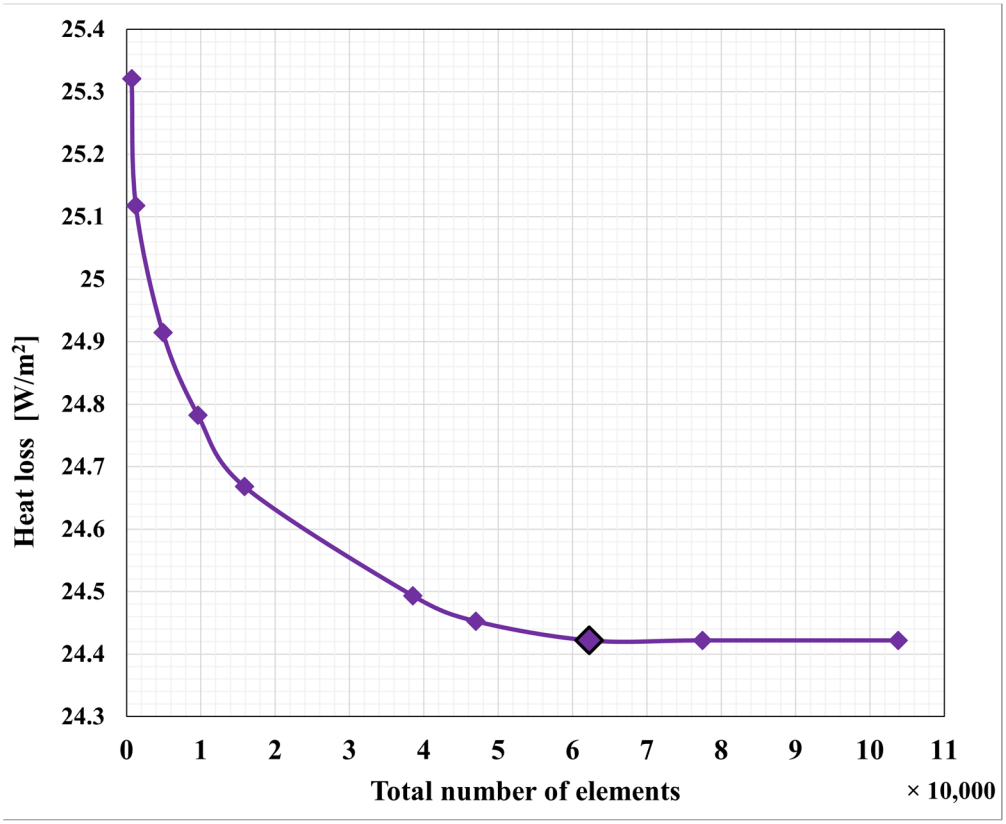

Figure 2. The mesh independence, where heat loss is taken as a function of the total number of elements.

3. Verification

Although analytical solutions provide valuable insights, they are sometimes limited to simplified cases, whereas simulation has several advantages, where it can deal with complex geometries and multi-layered structures that may be difficult to solve analytically, provides a detailed analysis of the temperature distribution across different layers, and allows convection and radiation to be incorporated in a more flexible manner. To make the numerical validation we have performed a comprehensive numerical verification of both convection and radiation conditions, in addition to conduction.

3.1. Verification in a Simple Case

Heat transfer by conduction verification proceeds by analyzing the heat flux rate across a wall consisting of three layers: wood, steel, and insulation with thicknesses 0.01 m, 0.006 m, and 0.02 m respectively with the material properties given in Table 1. Assuming indoor and outdoor temperatures of 22 °C and −8 °C, respectively.

- Analytical solution

The thermal transmittance, denoted as U, plays a crucial role in heat transfer analysis. It is based on Fourier's law of heat conduction and is defined by the following expression:

$$q = U\,\Delta\,T \tag{15}$$

where the variables are designed as follows:

Heat Flux Density (q): This represents the local heat transfer rate per unit area (measured in W/m^2) [33].

Temperature Difference (ΔT): It reflects the temperature gradient across the system (measured in kelvin, K).

$$U = \frac{1}{L_1/k_1 + L_2/k_2 + L_3/k_3} \tag{16}$$

Material Properties:

Thickness (L): The thickness of the material (measured in meters, m).

Thermal Conductivity (k): The material's ability to conduct heat (measured in W/m·K).

The overall heat transfer coefficient is then calculated as follows:

$$U = 1/(0.01/0.12 + 0.006/60.5 + 0.02/0.038) = 1.640021\ W/m^2K$$

The heat flux can be then calculated simply as follows:

$$q = 1.640021\ [W/m^2K] \times (295 - 265)\ [K] = 49.20063\ W/m^2$$

- Simulation solution

To validate the accuracy and reliability of our computational results, we perform a comparison with the previous analytical calculation. By assessing the agreement between the two approaches, we ensure the robustness of our numerical solution. Finally, we obtained q = 49.2006 W/m^2 using Ansys Fluent, which is the same as the result of the analytical calculation, q = 49.20063 W/m^2. Figure 3 shows the contour of the temperature and the average heat flux across the wall.

3.2. Verification of Convection and Radiation

Heat transfer by convection and radiation validation proceeds by investigating a two-dimensional (2D) cavity consisting of two layers of metal separated by an air gap. To facilitate the comparison with the reference study [34,35] containing non-dimensional results, two Rayleigh numbers based on two characteristic dimensions of 0.021 m and 0.097 m are studied as shown in Figure 4 and Tables 2 and 3. The properties of the air at the average temperature T_{mean} = 293.5 K are constant, as shown in Table 4, while the density varies according to the Boussinesq model.

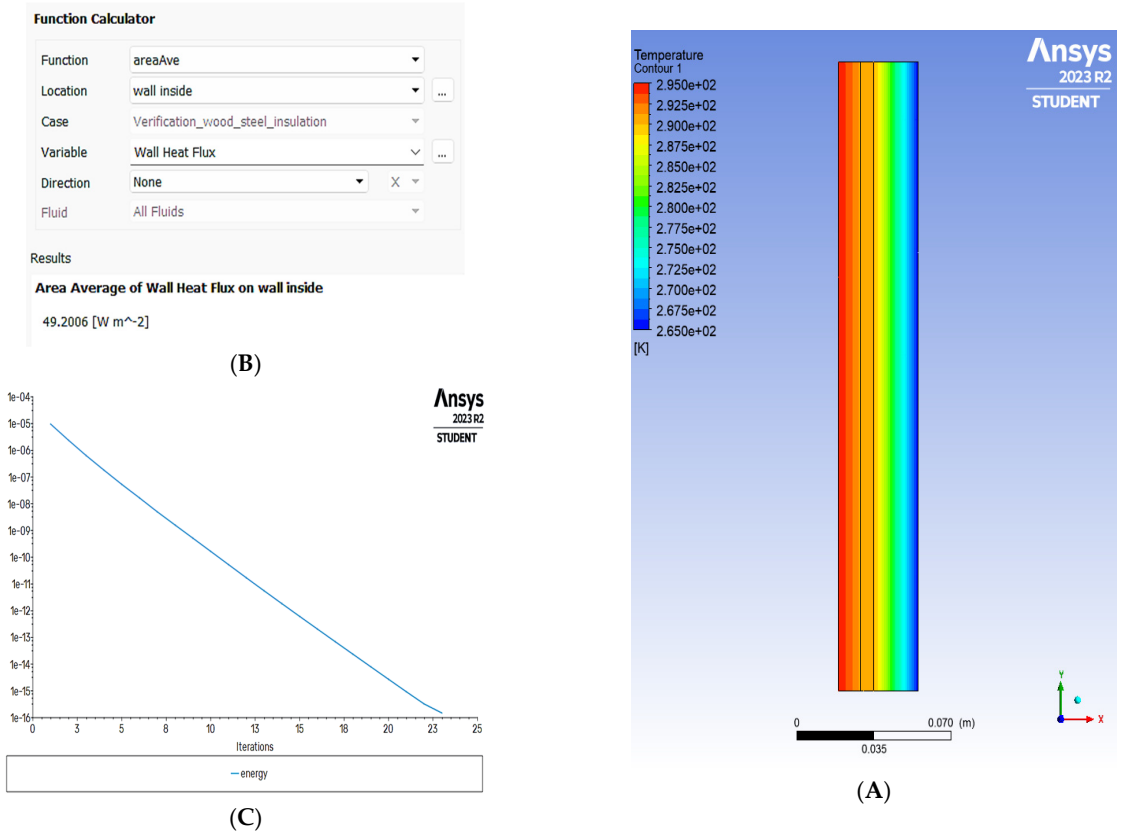

Figure 3. (**A**) The contour of the temperatures, (**B**) the average heat flux across the wall, and (**C**) the residual solution of the energy which is very small.

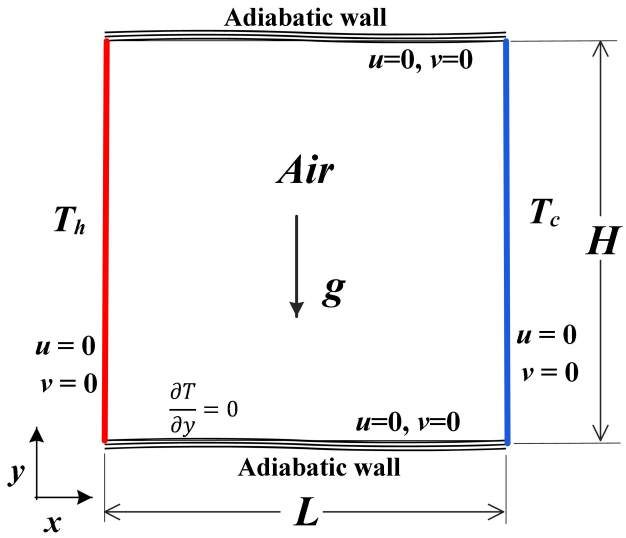

Figure 4. The studied 2D configuration with its boundary conditions.

Table 2. Rayleigh numbers depending on the characteristic length *L*.

Ra	*L* (m)	*H* (m)	*AR* = *H*/*L*
10^4	0.021	0.021	1
10^6	0.097	0.097	1

Table 3. Boundary conditions of the examined cavities.

The Walls	Wall Properties					
	Boundary Conditions		Emissivity ε			
Cold	T_c = 288.5 K	No slip, $u = 0$, $v = 0$	0	0.4	0.8	1
Hot	T_h = 298.5 K					
Adiabatic	$\partial T/\partial y = 0$					

Table 4. The physical properties of the air at average temperature T_{mean} = 293.5 K.

Name	Symbol	Value	Unit
Density	ρ	1.232	kg/m^3
Thermal conductivity coefficient	k	0.0249	W/(m·K)
Kinematic viscosity	v	1.43×10^{-5}	m^2/s
Dynamic viscosity	μ	1.761×10^{-5}	kg/(ms)
Specific heat	c	1008	J/(kg K)
Thermal diffusivity	α	2×10^{-5}	m^2/s
Thermal expansion coefficient	β	0.0034	K^{-1}
Prandtl number	Pr	0.71	

Dimensionless results are presented so that they can be compared with the dimensionless results documented in the literature [34,35], as shown in Figure 5 that provide radiation and convection modeling results for four values of radiation emissivity ε. As can be seen from Table 5, the study's results indicate a strong agreement between the computed Nusselt numbers Nu and the literature data. These allow us to conclude that this numerical approach can be considered valid.

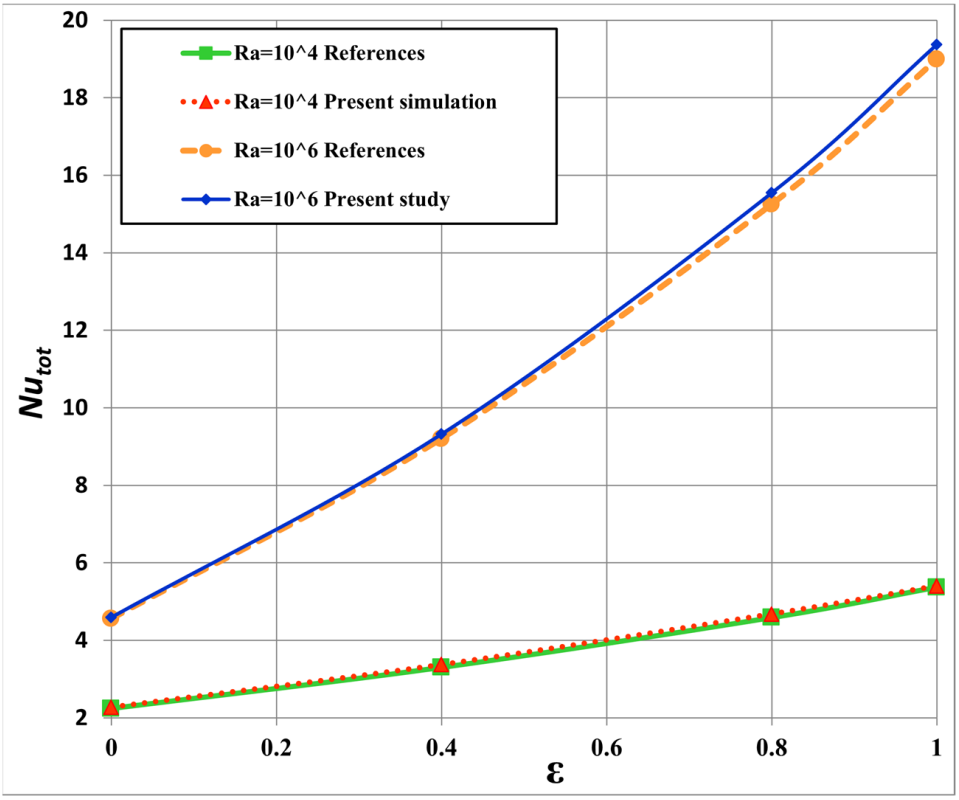

Figure 5. Comparison of the total Nusselt numbers according to the emissivity for the Rayleigh numbers 10^4 and 10^6 with the references [34,35].

Table 5. Comparison between the present simulation and the results in references [34,35] at Nu_{tot}.

ε	Nu_{tot}					
	$Ra = 10^4$			$Ra = 10^6$		
	Ansys Simulation	**Reference**	**Relative Error (%)**	**Ansys Simulation**	**Reference**	**Relative Error (%)**
0	2.277	2.25	1.19	4.59	4.56	0.843
0.4	3.37	3.30	2.013	9.32	9.207	1.288
0.8	4.68	4.59	1.93	15.54	15.25	1.935
1	5.40	5.37	0.545	19.37	18.99	2.025

4. First Round of Simulation and Optimization

4.1. Ansys Workbench

In the first phase of the research, we simulate the heat loss through the wall by Ansys for three types of gases, namely argon, air, and CO_2 with up to 20 layers and three thicknesses for the gas layer (5, 7.5, and 10 mm, which are represented at the top, middle, and bottom of the symbol). The results, which are presented in Figure 6 indicate that argon gas outperformed the other gases in all cases. The difference between argon and air is large, thus we exclude air from further investigations. Although argon is just slightly better than CO_2, it is cheaper as well, where the total cost of each wall model was calculated by determining the volume of each material used and its price per cubic meter from Table 1, thus the remaining part of the study will focus solely on argon gas.

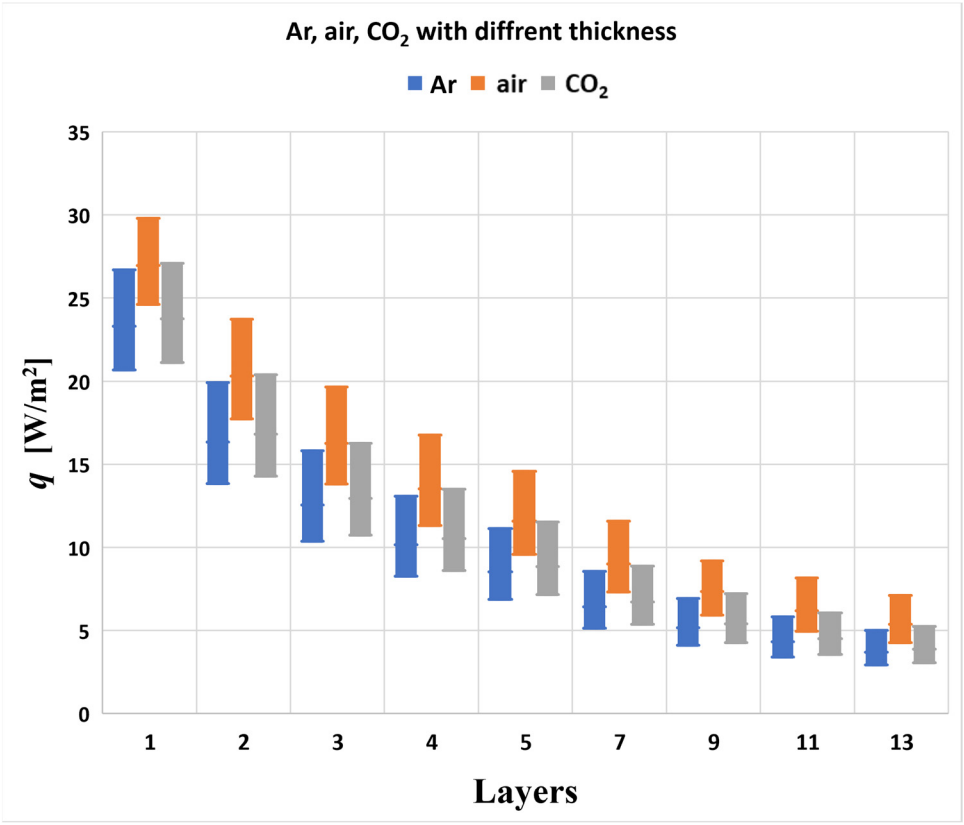

Figure 6. The experiment evaluates heat transfer on a uniform wall using three different types of gases and three different gas layer widths under identical conditions.

Ansys Workbench also enables designers to efficiently optimize performance and cost parameters using statistical techniques such as Design of Experiments (DOE). Additionally,

Ansys Workbench has a module for fluent flow and thermal analysis, which enables the execution of steady-state thermal simulations [36].

Based on the experimental design that the Minitab program recommended, we used Ansys to carry out 39 experiments, with 13 runs for each of the three argon layer thicknesses. In each run, we incrementally increased the number of argon layers by 2, ultimately reaching 26 layers. This approach allowed us to investigate the effects of multiple variables, including total wall thickness and the number of argon layers. The wood and steel layers in the inner part of all models, as well as the outer steel layer and insulator, were kept constant. The number of argon layers was varied, with the plastic layer having a constant thickness of 2 mm. The argon layers had three thicknesses (5, 7.5, and 10 mm), and the total wall thickness increased as the number of argon layers increased. The output data obtained by Ansys are used in Minitab, which is described in the next section.

4.2. Minitab

Minitab is a statistical program that provides a set of techniques for statistical analysis, including response surface methodology (RSM). The Design of Experiments (DOE) interface in Minitab allows users to create response surface designs, evaluate experimental results, and determine the most appropriate factor configurations. RSM is a set of advanced DOE methods that help understand and improve the response variable [37]. Response Surface Methodology (RSM) was employed to optimize the response of our system. RSM is a collection of statistical and mathematical techniques useful for developing, improving, and optimizing processes. The analysis was conducted using Minitab software, which facilitated the design and analysis of the experiments. A central composite response surface experiment was designed to examine the factors affecting our response variable. The factors included the number of plastic layers, the thickness of plastic layers, and the type of gas. The design allowed us to model the curvature in the data and identify the optimal settings for these factors. Data were collected in Ansys Fluent for the experimental design and input into Minitab. The software was used to perform the following steps:

- Creating the Response Surface Design: We selected the range of factors.
- Running the Experiments: The experiments were conducted, and the response values were recorded.
- Analyzing the Response Surface Design: We analyzed the design by selecting the terms, options, graphs, and storage in Minitab. This included generating coded coefficients, model summaries, ANOVA tables, regression equations, Pareto charts, and residual plots. It was found that argon gas was the best according to cost and heat loss compared to CO_2 and air; therefore, the study continued using argon. Table 6 shows the errors for the heat loss and cost in the equations. Figure 7 present Surface plot of heat loss and cost.

Table 6. Model summary R^2.

	***S* (Standard Error)**	**R-sq**
q [W/m^2]	0.000938360	90.78%
Cost [$]	0.0000001	100.00%

While we need only the equations for the data to use it in optimization tool.

$$Q = 8.222 - 0.0702\ \mathrm{N} - 0.0095\ \mathrm{T} + 0.00290\ \mathrm{N}^2 + 0.000078\ \mathrm{T}^2 \quad (17)$$

$$Cost = 74.6294 + 3.18599\ \mathrm{N} \quad (18)$$

where q: heat loss [W/m^2], N: number of plastic layers, and T: thickness of plastic layers [m].

Based on our analysis, the cost of plastic is primarily influenced by the number of plastic layers [$/m^3]. The program assumes a linear relationship between the number of plastic sheets and the overall cost, as the thickness has a minimal impact on the price.

Using RSM in Minitab allowed us to efficiently explore the relationships between multiple factors and the response variable. The optimized settings identified through this analysis can be used to improve multi-layer walls. This methodology proves to be a powerful tool for process optimization and can be applied to various fields of study.

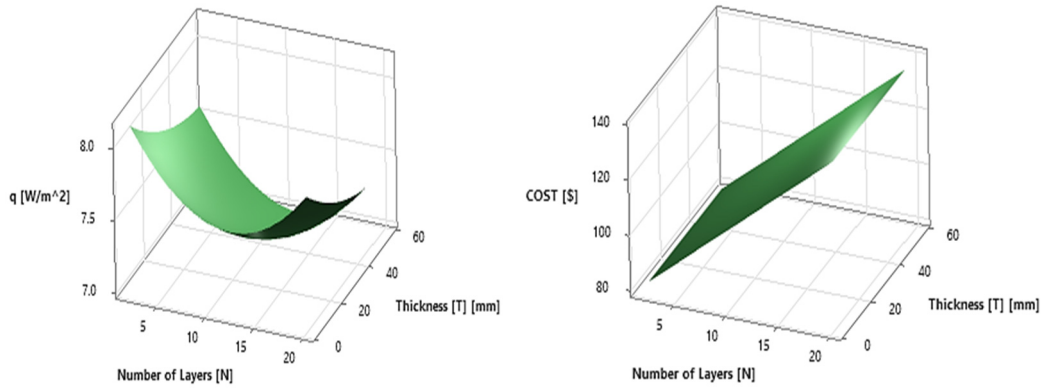

(**A**) (**B**)

Figure 7. Surface plots of heat loss (**A**) and cost (**B**) with the number of layers and thickness of argon gas.

4.3. Isight

Isight 2019 version 6.3 is a software framework that offers a collection of tools for integrating processes and optimizing designs. It is used to streamline the laborious and repetitive process of analytical design by incorporating design and simulation models generated by several CAD, CAE, and other software tools. Products are improved by using statistical methodologies, such as DOE or Design for Six Sigma, to optimize them in terms of performance or cost metrics using Isight [38]. This results in time savings and improved product outcomes. It is advantageous for minimizing time and expenses, enhancing product dependability, and attaining a competitive edge [39]. Most of the tools, such as NLPQLP and HOOKE JEEVES, were tried, and the PSO tool was found to be the best.

4.4. Particle Swarm Optimization (PSO)

An optimization model was developed using the Isight program, leveraging Particle Swarm Optimization (PSO) algorithms. The equations from the previous section were formulated to accurately represent the system's parameters and constraints. By integrating these equations into the Isight environment, PSO was utilized to efficiently explore the solution space. Initially, the optimization technique values were set by default; see Table 7. Subsequently, the variables are argon number layers and thickness of argon layer, and the objective were defined as the heat loss and the cost of the wall, with the direction of the optimization aiming to minimize both, with no constraints present in this problem. This method allowed for the fine-tuning of model parameters, resulting in significant improvements in performance and efficiency.

We developed a regression equation for the heat loss and cost of the models by utilizing MRS and the data produced by the first round of Ansys simulation. Then we used this regression equation as a function of heat loss and cost to calculate the optimum design parameters [40] by using the optimization tool PSO in Isight program. The input parameters used in PSO included the range of argon layer counts (0–50) and the range of thickness of each individual argon layer (0–12 cm), while the output parameters included the heat loss and the cost of the wall. There are no constraints imposed on the variables, except that the lower bound for the objects is set to zero to prevent negative values. Thus, after running 500 iterations to ensure the feasibility of a proposed design within its constraints,

the objective function defines the optimization goal, such as cost minimization. The optimization process is illustrated in the flow chart shown in Figure 8. Penalty functions add costs for constraint violations, guiding the process towards feasible solutions see Table 8. The optimal parameters are thickness of the argon layer, the number of layers, heat loss through the wall and the cost of the wall are determined using the PSO method as shown in Table 9.

Table 7. The optimization technique options.

Option	Value
Maximum Iterations	50
Number of Particles	10
Inertia	0.9
Global Increment	0.9
Particle Increment	0.9
Maximum Velocity	0.1
Max Failed Runs	5
Failed Run Penalty Value	1.0×10^{30}
Failed Run Objective Value	1.0×10^{30}

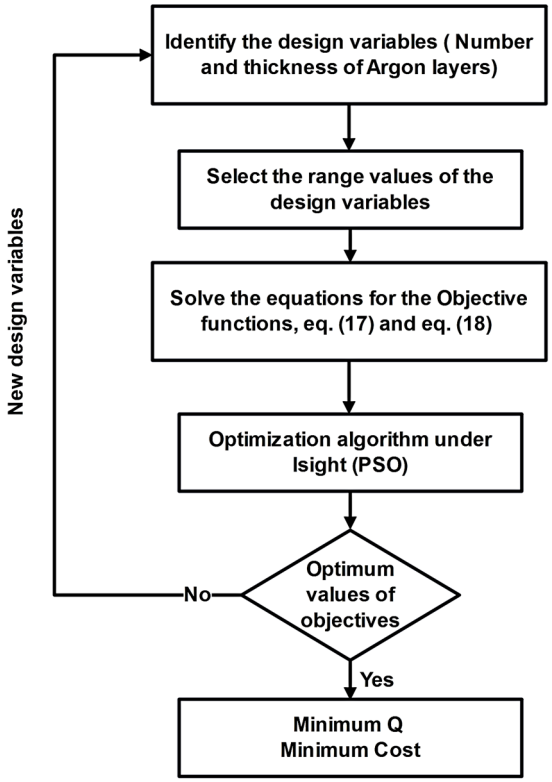

Figure 8. The steps of the optimization process.

Table 8. The optimum design points according to the PSO optimization tool.

Gas	Layers	Thickness of Gas [mm]	q [W/m^2]	Cost per Cubic Meter [$]	Design Feasibility	Objective and Penalty	Objective Function	Penalty Function
Argon	12	8	8.45	5	9	13.49505	13.49505	0

Table 9. The results showing the optimum design parameters for argon gas according to PSO optimization tool.

Gas	Layers	Thickness of Gas [mm]	Total Thickness of Wall [mm]	q [W/m^2]	Cost per Cubic Meter [$]
Argon	12	8	154	8.45	5

So based on the first round of Ansys simulation and a regression equation, PSO gave that the economic optimum of the number of the plastic layers is 11. We decided not to stop here but to perform a second round of Ansys Fluent simulation with only one variable, which is the number of plastic layers, and maintain the total wall thickness as a constant parameter. The goal is to determine the optimal number of argon layers from a thermal as well as economical point of view. Although Ansys is slower, it is more accurate than optimization based on regression equations; thus, the result reinforced by the second round will be more reliable.

5. Second Round of Simulation and Optimization

We perform a steady-state thermal analysis in Ansys, where the wood layer and steel layer in the inner part of all models were kept constant, as well as the outer steel layer and insulator, considering that the wall width is fixed and equal to 15.4 cm. The number of plastic layers varied, and hence the number of gas layers, since the number of gas layers is equal to the number of plastic layers plus one. The study involved a maximum of 31 layers (32 argon layers) with a fixed thickness of plastic of 2 mm. The thickness of the individual gas layers decreases from 0.118 to 0.00175 m with an increasing number of plastic layers. It has two reasons: the total space for gas is decreasing, and this is cut by more and more pieces with an increasing number of plastic layers. The boundary condition used on the inner and outer surfaces is based on the coldest day in Miskolc City (Hungary) during the past winter [41]. The convection heat transfer coefficient for the outside surface hc_{os} as a function of air velocity v [m/s] is calculated from the equation below [42], and the used values for the boundary are presented in Table 10.

$$hc_{os} = 0.6 + 6.64\sqrt{v} \tag{19}$$

Table 10. The convection, radiation, and temperature characteristics on both sides of the wall components [42,43].

	$h_c \left[\frac{\mathrm{W}}{\mathrm{m^2K}}\right]$	ε	T
Outer surface	15	0.9	265 K ≈ -8 °C
Inner surface	8.5	0.9	295 K $\approx$ 22 °C

The results are calculated for the multi-layer outside walls, first with only one thickness of insulation, which is given in Section 3. We calculate the results first without and then with reflective layers made of aluminum with an emissivity 0.05. We compare these with the three types of standard walls. After that, we increase the insulation thicknesses for the further optimization of the multi-layer wall and calculate the new results.

5.1. The Reference Walls

We made simulations for three types of standard walls, shown in Figure 1A,B. We calculate the heat loss through them, and after that, as will be presented in the next section, we compare them with the new multi-layer walls. Figure 9 shows the temperature contour for two types of reference walls. One can see that the concrete wall with insulation has a sharp temperature gradient; therefore, it provides better thermal resistance than the brick wall. This means that the insulated concrete wall is more effective in minimizing heat transfer.

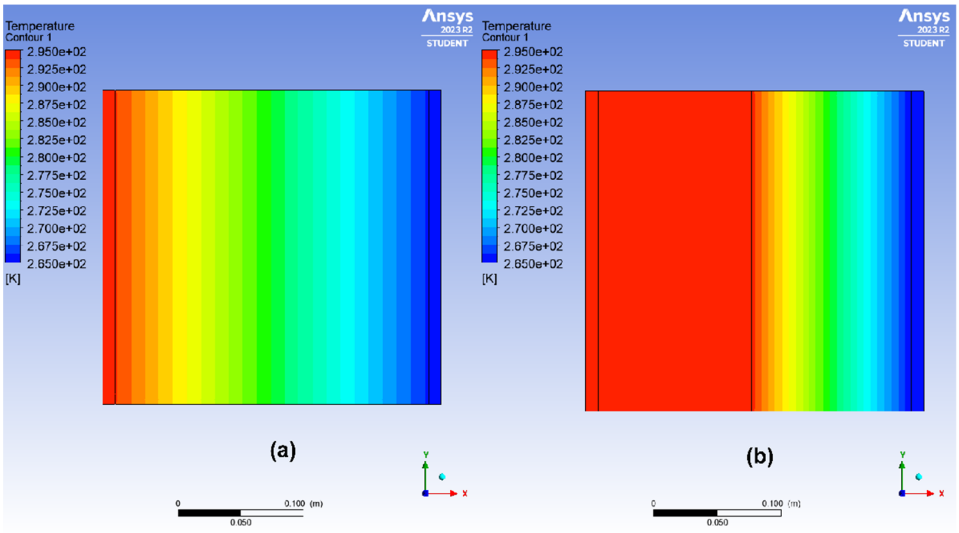

Figure 9. The temperature distribution contours in kelvin for two types of normal walls: (**a**) a brick wall and (**b**) a concrete wall with insulation.

5.2. Multi-Layer Wall Without Reflective Layers

Figure 10 illustrates the relationship between the heat loss and the number of plastic layers. One can see that when the number of plastic layers increases, the heat loss decreases until there are 21 layers of plastic. The reason for this is that increasing the number of plastic layers decreases the radiation heat transfer in addition to decreasing the convection between the layers because the spaces will be smaller and smaller, which does not allow the fluid to move inside the spaces [44]. However, after 21 layers, the heat loss starts to increase again due to the plastic layers being more effective thermal conductors than argon layers. Therefore, there is an optimum number of layers, which is 21 layers of plastic. Furthermore, we plot the heat loss for two insulated reference walls as straight lines. One can see the multi-layer wall achieves a lower heat loss than both reference walls when it has more than about 10 plastic layers. In the case of a normal brick wall without insulation the heat loss is 176.7 [kWh/m^2], thus it cannot be put into the same figure.

We now consider the economic side [45] of the optimization. One can save a great deal of money because a larger number of plastic layers decreases the radiation heat transfer. However, one must invest more because more layers mean a higher cost of investment, as plastic is more expensive than argon. As the number of plastic layers starts to increase, the total cost substantially decreases. However, this decrease slows down and then turns into an increase primarily due to the heightened investment in plastic layers. Consequently, the economic optimum is different from the thermal optimum. We obtained that the number of plastic layers for optimal performance is 11 (instead of 22), as shown in Figure 11. Table 11 shows the economic calculations for the multi-layer wall. The heating loss still decreases noticeably, but the total savings decrease because the cost increases linearly with the number of layers. If we increase the number of layers, the life-cycle savings on heating rapidly increase at first but then go down after 11 plastic layers.

One can see from Table 11 based on the second round of Ansys simulation that there is good agreement in the case of economic optimal design parameters of the number of argon layers with the previous calculation of PSO.

A comparison between the multi-layer walls can be made by plotting the temperature as a function of the position for different numbers of plastic layers, as shown in Figure 12. One can notice that if the number of layers is larger, the temperature gradient and therefore the heat flux in the wood (left side) and EPS (right side) layers are smaller. Figure 13 shows the temperature distribution contour in kelvin for two types of multi-layer walls, namely, without a plastic layer and with one plastic layer, compared to the thermal and economic optimum cases.

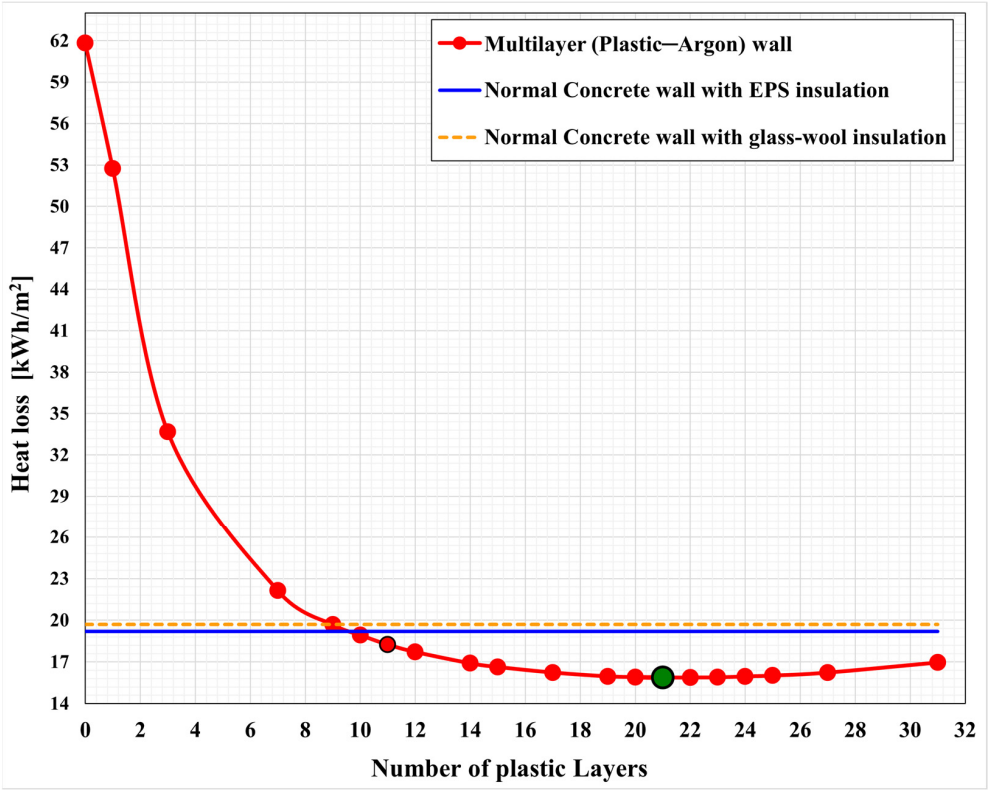

Figure 10. The heat loss as a function of the number of plastic layers for multi-layer walls compared to the insulated reference walls.

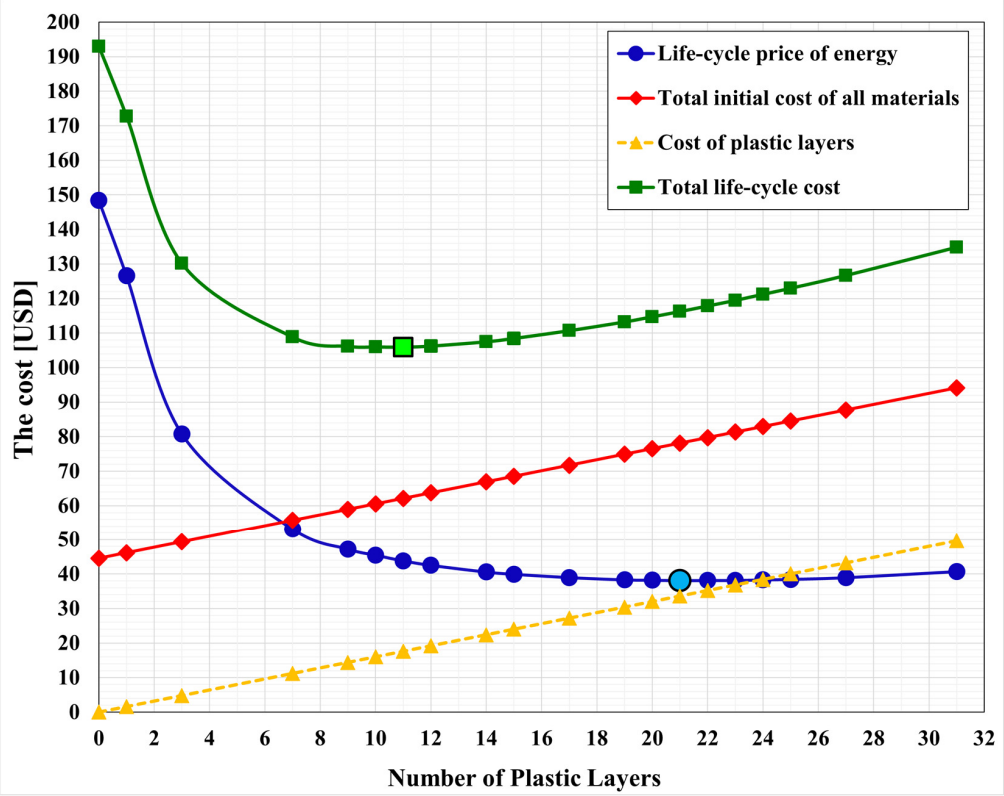

Figure 11. Economical quantities as a function of the number of plastic layers. The optimum numbers of plastic layers according to thermal and economic optimization are highlighted.

Table 11. The key quantities as a function of the number of plastic layers. The rows containing the optimum numbers of plastic layers are highlighted.

No. of Argon Layers	No. of Plastic Layers	Heat Loss [W/m^2]	Annual Heat Energy Loss [kWh/m^2]	Life-Cycle Price of Energy [USD]	Total Initial Cost [USD]	Total Life-Cycle Cost [USD]
1	0	28.63	61.80	148.41	44.54	192.94
2	1	24.42	52.75	126.60	46.14	172.74
4	3	15.60	33.68	80.83	49.34	130.17
8	7	10.25	22.14	53.12	55.74	108.85
10	9	9.11	19.68	47.236	58.93	106.17
11	10	8.77	18.94	45.45	60.54	105.99
12	**11**	**8.45**	**18.25**	**43.80**	62.14	105.94
13	12	8.20	17.71	42.52	63.74	106.26
15	14	7.82	16.90	40.57	66.94	107.5
16	15	7.70	16.64	39.93	68.54	108.47
18	17	7.52	16.24	38.97	71.74	110.71
20	19	7.39	15.96	38.31	74.94	113.24
21	20	7.367	15.91	38.19	76.54	114.73
22	**21**	**7.350**	**15.87**	**38.10**	78.14	116.24
23	22	7.352	15.88	38.11	79.74	117.85
24	23	7.356	15.89	38.137	81.34	119.47
25	24	7.388	15.96	38.30	82.94	121.24
26	25	7.41	16.02	38.44	84.54	122.98
28	27	7.51	16.23	38.96	87.74	126.69
32	31	7.85	16.96	40.70	94.14	134.84

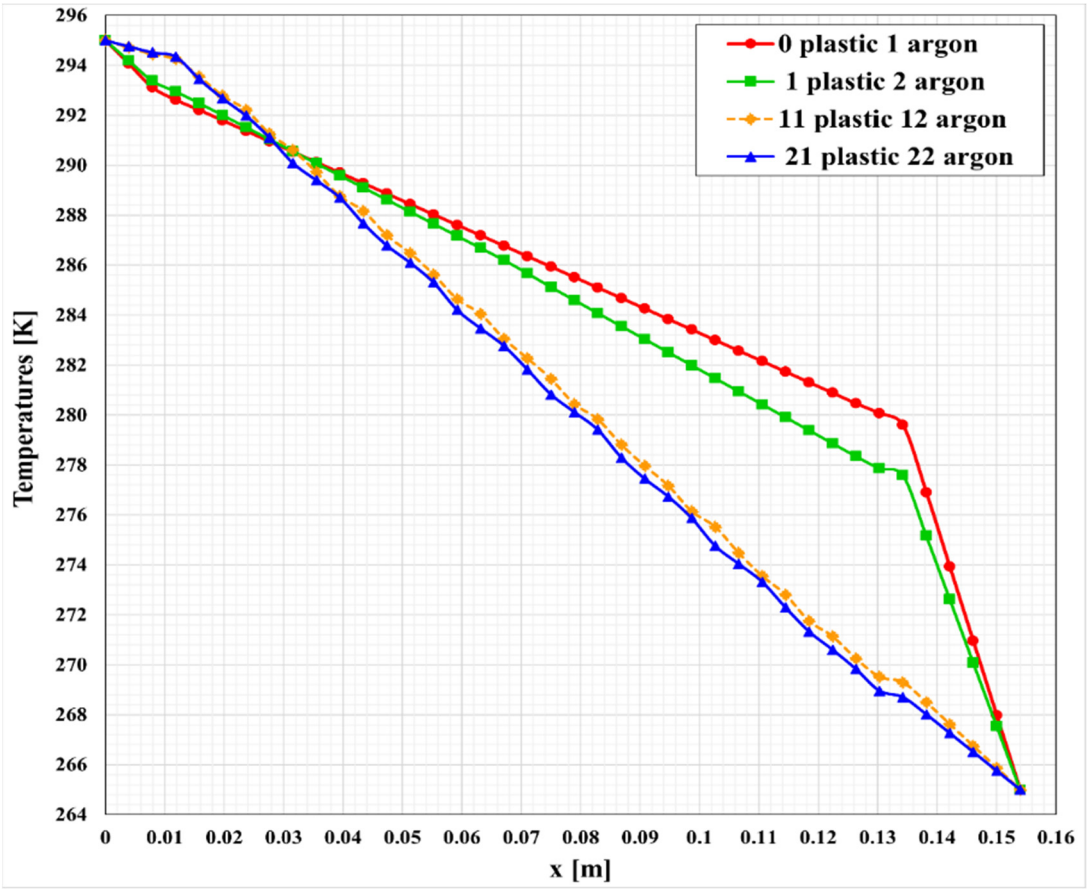

Figure 12. The temperatures in [K] as a function of the x coordinate for four types of multi-layer walls, including the two optimum cases.

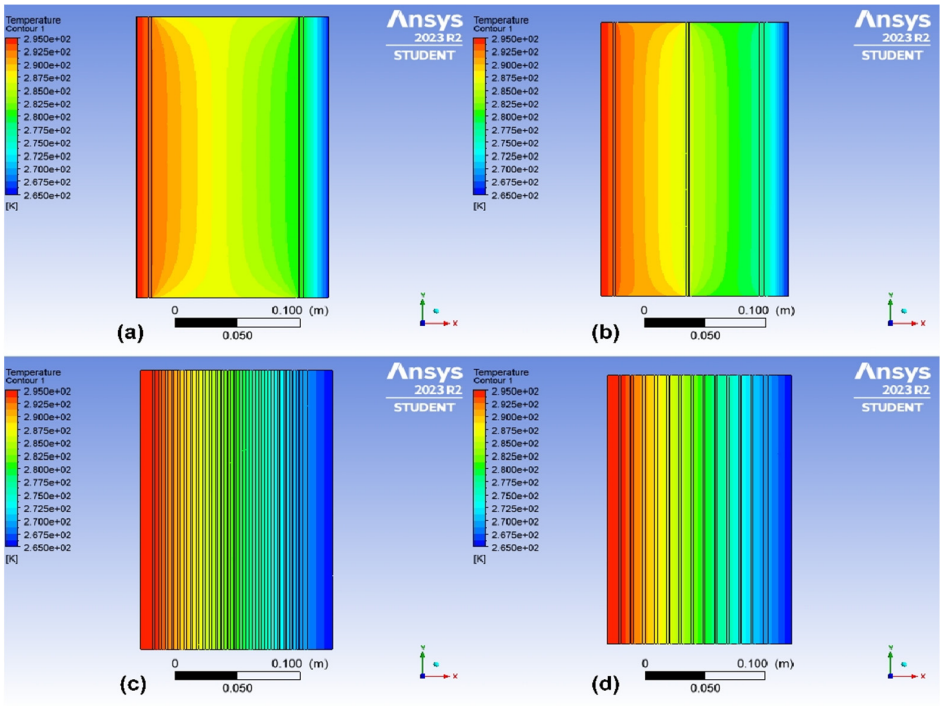

Figure 13. The temperature distribution contours in kelvin for two types of multi-layer walls, namely, (**a**) without a plastic layer and (**b**) with one plastic layer, compared to the (**c**) thermal and (**d**) economic optimum cases.

5.3. Multi-Layer Wall with Reflective Layers

Now, we add aluminum foil to the plastic layers in addition to the inner surfaces of the steel layers to reflect the radiation, and in this case, we increase the price by adding the aluminum to the plastic. We note that the heat loss decreases because most of the radiation which goes across the argon layer is reflected due to the reflective layer. One can see from Figure 14 that after adding the foil aluminum layer, the optimum number of plastic layers is decreased to only one layer. The only negative effect of adding a layer of aluminum is that plastic with aluminum is harder to recycle. Figure 15 shows the temperature distribution contour in kelvin for the one plastic layer with a reflective layer compared to the one without a reflective layer. One can see that when the reflective layer is present, the middle layer is cooler, since radiative heat transfer is hindered. Moreover, the temperature gradients are smaller in this case in the wood and insulator layers. The comparison between the temperature distribution in the three multi-layer optimum walls compared to two types of reference walls is shown in Figure 16. One can see that the temperature in the normal brick wall has a significant decrease across the wall thickness due to the lack of insulation. However, in the normal concrete wall with EPS insulation, the temperature stays nearly constant at around 294 K, and after that, a sudden drop is caused by the presence of EPS insulation, significantly slowing down heat loss. In all multi-layer walls, we can see a slow but steady temperature drop, showing good insulation properties with a nearly steady gradient.

Table 12 shows the values of the key quantities for the optimum multi-layer walls compared to the reference walls.

We then make calculations with greater thicknesses of EPS insulation layer to approach the optimal multi-layer wall with and without a reflective layer. The reason for this, as we see from Table 12, is that the heat loss is further reduced by increasing the thickness of the insulator to the extent that the total life-cycle cost can be further decreased despite the increased cost resulting from increasing the thickness of the insulation. One can see that our wall is still cheaper and, at the same time, thermally better than the standard walls. Figure 17 shows the temperature distribution contours for the optimum cases.

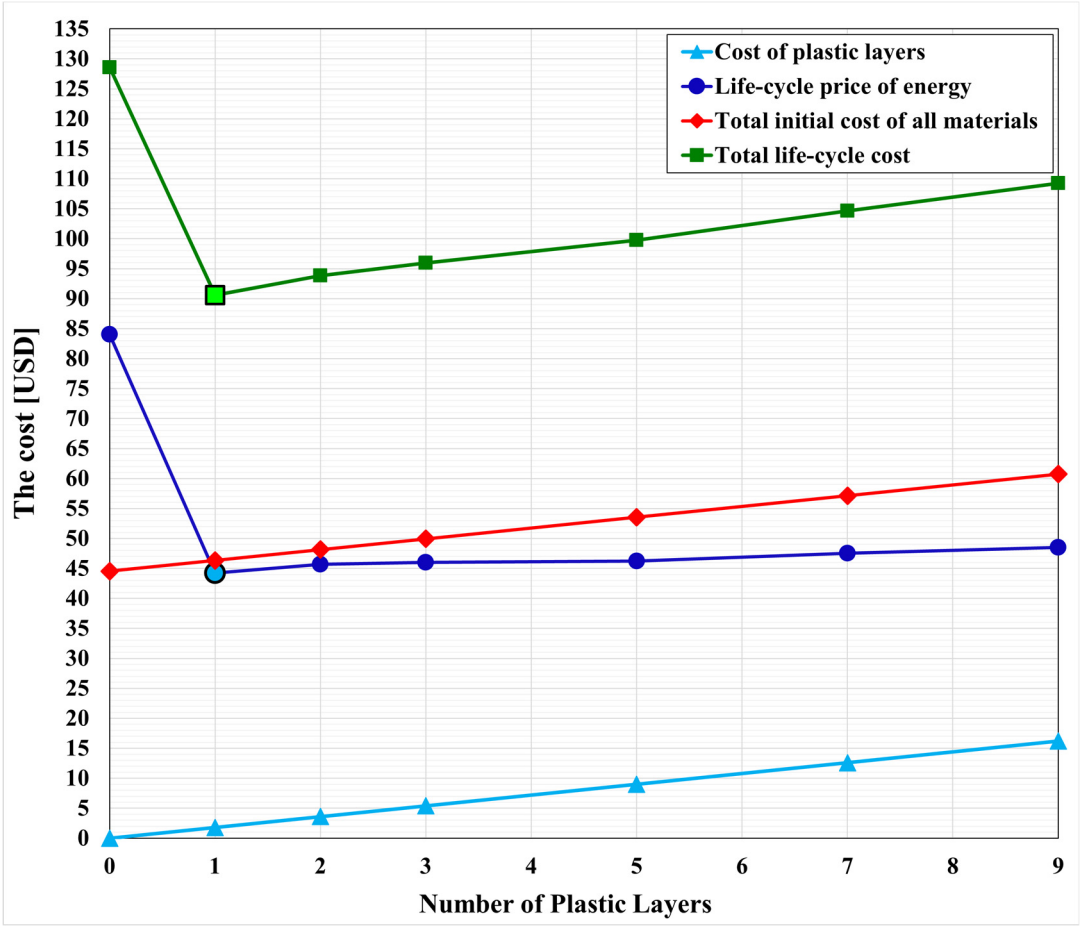

Figure 14. The optimum number of plastic layers in the case of a wall with reflective layers.

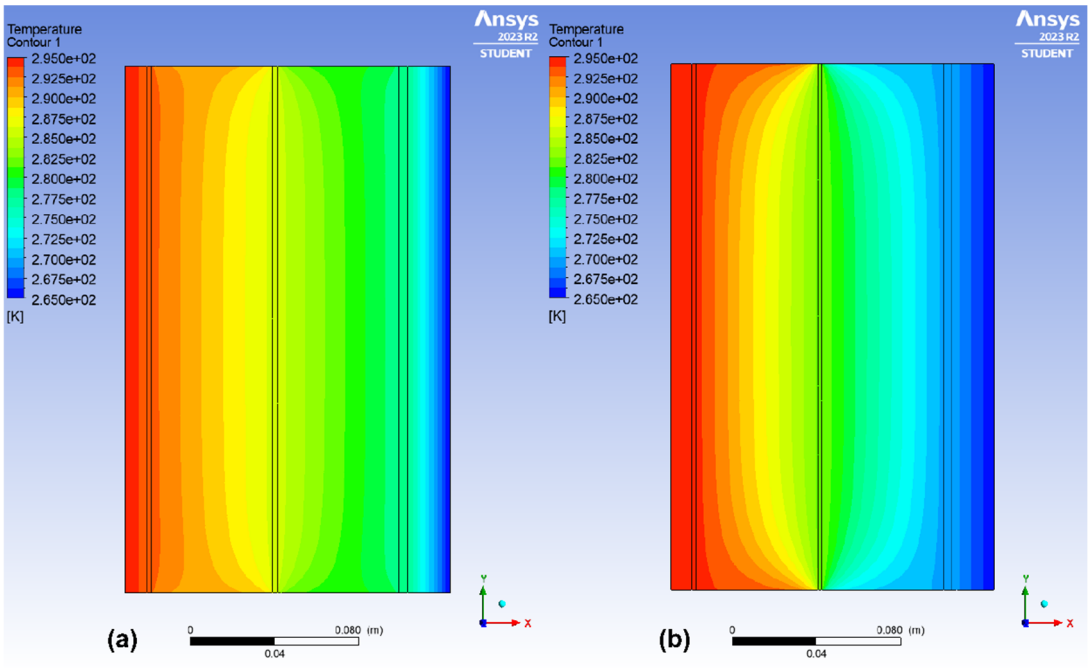

Figure 15. The temperature distribution contours in kelvin for two types of multi-layer walls: (**a**) one plastic layer without a reflective layer and (**b**) one plastic layer with a reflective layer.

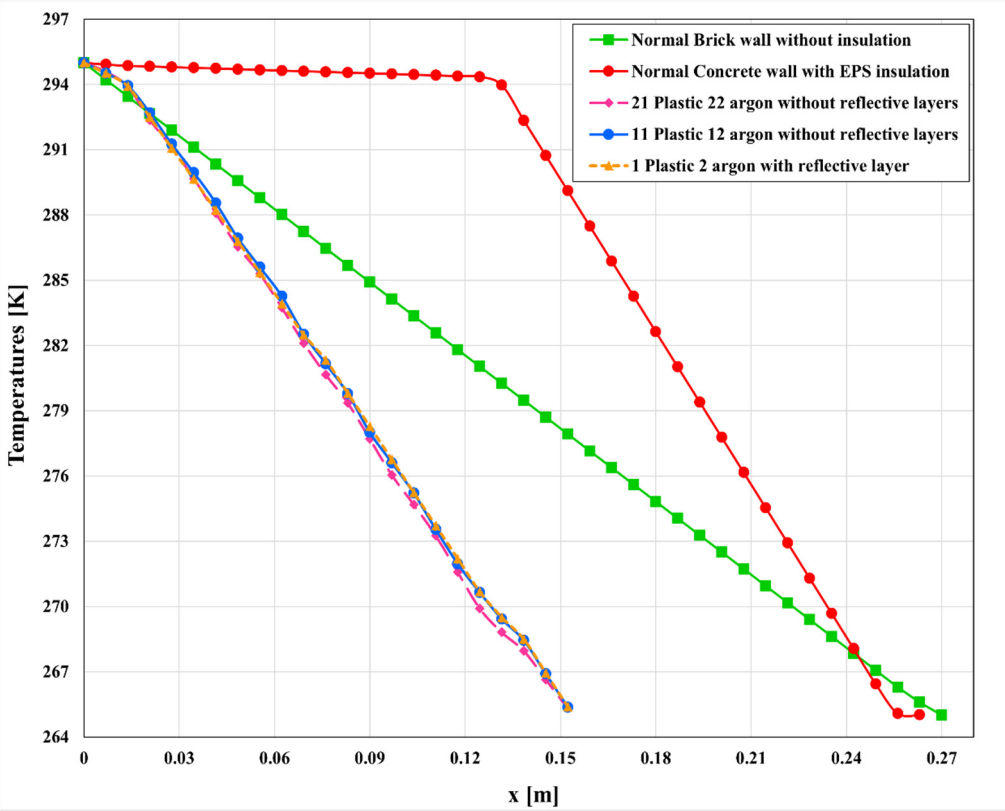

Figure 16. The temperatures in [K] as a function of the x coordinate for the three optimum walls compared to two types of reference walls.

Table 12. The final comparison between the optimum walls and the reference walls.

List of Walls	Materials	Insulation Thickness [m]	No. of Plastic Layers	Wall Type	Heat Loss [W/m^2]	Annual Heat Energy Loss [kwh/m^2]	Life-Cycle Price of Energy [USD]	Total Initial Cost [USD]	Total Life-Cycle Cost [USD]
Multi-layer without reflective layers	Wood, Steel, Argon, Plastic, EPS	0.02	11	Economically optimal	8.45	18.25	43.8	62.14	105.94
		0.03			7.9	17.07	40.98	63.10	104.08
		0.04			7.42	16.04	38.49	64.08	102.57
		0.02	21	Thermally optimal	7.35	15.87	38.1	78.14	116.24
		0.03			6.93	14.97	35.93	79.10	115.04
		0.04			6.56	14.17	34.02	80.08	114.10
Multi-layer with reflective layer		0.02	1	Thermally and economically optimal	8.53	18.43	44.22	46.34	90.56
		0.03			7.96	17.2	41.28	47.30	88.59
		0.04			7.46	16.12	38.7	48.28	86.98
Normal wall without insulation	Plaster, Brick, Cement			Reference walls	81.8	176.7	424.08	17	441.08
Normal wall with insulation	Plaster, Concrete, EPS, Cement	0.125			8.88	19.19	46.07	77.25	123.33
	Plaster, Concrete, Glass Wool, Cement	0.125			9.11	19.69	47.26	74.75	122

We note that in the price of the initial investment, we included the price of the materials, but not the price of construction, because it strongly depends on the technology and the price of labor. We think that if the container house is manufactured in series in a factory,

the manufacturing cost can be smaller than for standard walls, especially brick walls built manually by bricklayers.

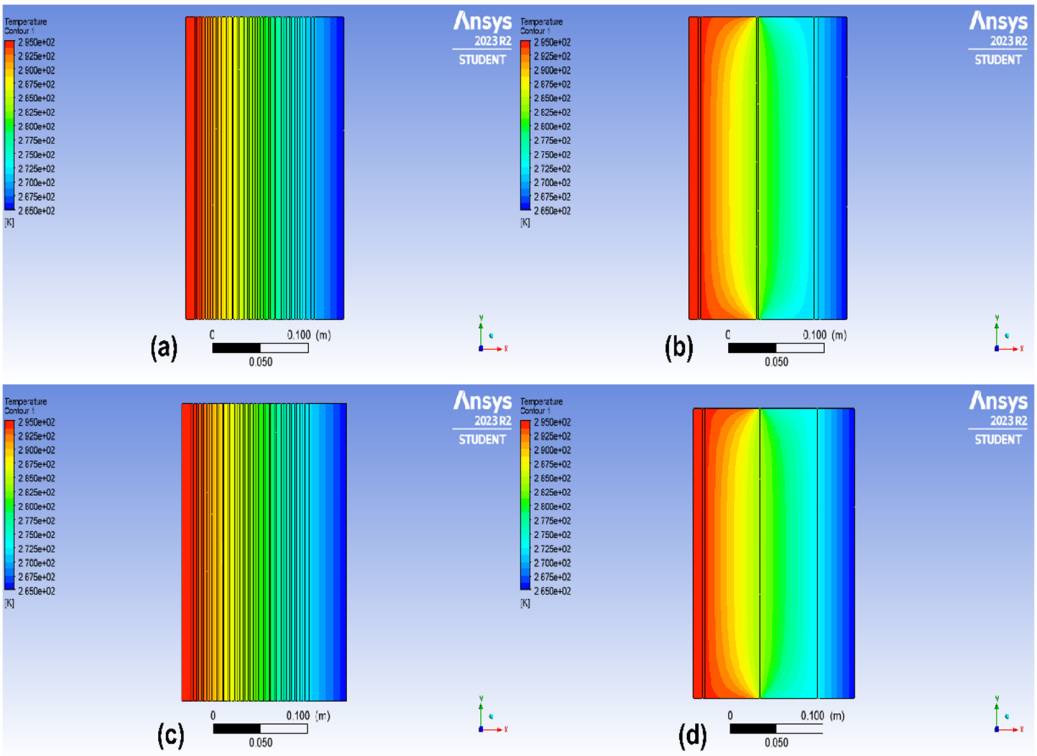

Figure 17. The temperature distribution contours in kelvin for the two types of thermally optimal multi-layer walls with different thickness of EPS insulation: (**a**,**b**) 0.03 m and (**c**,**d**) 0.04 m.

6. Conclusions

This research proposed a novel sandwich-structured wall for container houses containing argon gas and plastic layers to minimize heat loss during cold winters. Steel walls have good earthquake and fire resistance, and the double steel layers prevent leakage of the argon. We attempted to optimize the configuration and overall cost of wall construction, drawing comparisons to the performance of conventional walls associated with brick, concrete, and insulation. Additionally, the study investigates the phenomena related to the number of plastic layers in the gas-filled wall.

- We found that as the number of plastic layers increases, heat loss decreases due to reduced radiative heat transfer and limited convective movement of argon within the increasingly smaller spaces between layers. This trend continues until the wall comprises 21 layers of plastic. Beyond this point, heat loss begins to increase again as the conduction through the plastic layers becomes more significant than the insulating effect of the argon layers. In the case of 21 plastic layers, the initial investment is slightly larger than in the case of the standard walls. However, the heating load is much smaller, and this easily counterbalances the initial cost in 20 years.
- From the point of view of economic optimization, the finding is the following: while increasing the number of plastic layers can lead to substantial savings due to decreased radiation heat transfer, hence decreasing the heat loss, it also necessitates greater investment due to the high cost of plastic. Consequently, the total gain diminishes for walls with many layers. Furthermore, as the number of layers increases, conduction also increases, offsetting the decrease in radiative heat transfer. Therefore, the optimal number of plastic layers from an economic point of view is 11, which is fewer than if only thermal optimization is performed. Above this, the heat loss still decreases, but the life-cycle cost of housing starts to increase. Moreover, if a high-reflectivity layer

covers the plastic layer, only one layer is enough to decrease heat loss to the level of eleven plastic layers without this reflective layer. Hence, one layer with reflective coating minimizes the heat loss as well as the cost of housing. These two economic optimums—eleven plastic layers without and one plastic layer with reflective coating—perform better than the standard walls in initial investment, heating load, and total cost of housing as well. We found for an insulation thickness of 2 cm, the maximum total life-cycle savings are 335.14 and 350.52 USD, respectively, while the minimum savings are 16.06 and 31.44 USD, respectively, for multi-layer walls without and with reflective layers compared to conventional walls. The maximum amount of decrease in annual energy loss is 160.73 [kwh/m^2], while the minimum amount is 3.32 [kwh/m^2], for the multi-layer thermally optimal wall without reflective layers compared to conventional walls.

- These findings provide valuable insights for the design of energy-efficient and cost-effective multi-layered walls.
- The importance of this research lies in producing new multi-layer walls for container houses capable of resisting earthquakes, significantly reducing heat loss through such walls, and, at the same time, reducing the overall cost compared to conventional brick or concrete walls.

After the completion of this paper, we plan to perform long-term transient calculations using real weather data, and based on these, optimization for different climates will be carried out.

Author Contributions: Conceptualization, resources, and supervision: E.K.; methodology: E.K., I.O. and A.H.A.; software and visualization: I.O. and A.H.A.; validation: I.O. and A.H.A.; investigation: I.O.; writing—original draft preparation: I.O. and A.H.A.; writing—review and editing, I.O., A.H.A. and E.K. All authors have read and agreed to the published version of the manuscript.

Funding: The research was funded by the EKÖP-24-4-I, supported by the University Research Scholarship Program of the Ministry for Culture and Innovation through the National Research, Development, and Innovation Fund.

Data Availability Statement: The data are available from the authors on reasonable request.

Conflicts of Interest: The authors declare no conflicts of interest.

References

1. Cozzarini, L.; Marsich, L.; Ferluga, A.; Schmid, C. Life Cycle Analysis of a Novel Thermal Insulator Obtained from Recycled Glass Waste. *Dev. Built Environ.* **2020**, *3*, 100014. [CrossRef]
2. Mawardi, I.; Aprilia, S.; Faisal, M.; Ikramullah; Rizal, S. An Investigation of Thermal Conductivity and Sound Absorption from Binderless Panels Made of Oil Palm Wood as Bio-Insulation Materials. *Results Eng.* **2022**, *13*, 100319. [CrossRef]
3. Alsaffar, A.K.K.; Alquzweeni, S.S.; Al-Ameer, L.R.; Ali, A.H.; Mohamed, A.; Aldaihani, H.M.; Reham, A.; Al-Ansari, N.; Al-Hashimi, O.; Shubbar, A.; et al. Development of Eco-Friendly Wall Insulation Layer Utilising the Wastes of the Packing Industry. *Heliyon* **2023**, *9*, e21799. [CrossRef]
4. Ndanduleni, A.U.C.; Radebe, T.B.; Huan, Z. Reduction of Temperature Fluctuation in a South African Shack House Using Phase Change Material Insulation. *Build. Environ.* **2023**, *241*, 110376. [CrossRef]
5. Calama-González, C.M.; Escandón, R.; Alonso, A.; Suárez, R.; León-Rodríguez, Á.L.; Sánchez-Ostiz Gutiérrez, A.; Arriazu-Ramos, A.; Monge-Barrio, A. Thermal Insulation Impact on Overheating Vulnerability Reduction in Mediterranean Dwellings. *Heliyon* **2023**, *9*, e16102. [CrossRef] [PubMed]
6. Juanicó, L.E. Thermal Insulation of Roofs by Using Multiple Air Gaps Separated by Insulating Layers of Low Infrared Emissivity. *Constr. Build. Mater.* **2020**, *230*, 116931. [CrossRef]
7. Mavromatidis, L.E.; Bykalyuk, A.; El Mankibi, M.; Michel, P.; Santamouris, M. Numerical Estimation of Air Gaps' Influence on the Insulating Performance of Multilayer Thermal Insulation. *Build. Environ.* **2012**, *49*, 227–237. [CrossRef]
8. Noaman, D.S.; El-Ghafour, S.A. Holistic Design of Energy-Efficient Temporary Houses: Meeting Ventilation, Heating, Cooling, and Lighting Demands. *J. Build. Eng.* **2024**, *86*, 108534. [CrossRef]
9. Abdullah, H.K.; Faraj, S.H. Experimental Study for the Effect of Air Gap in Building Walls on Heat Gain Reduction. *Mater. Today Proc.* **2022**, *61*, 1043–1051. [CrossRef]

10. Borelli, D.; Cavalletti, A.; Cavalletti, P.; Peshku, J.; Tagliafico, L.A. A Methodology to Evaluate the Optimal Insulation Thickness for Heating and Cooling Needs in Different Climatic Zones for Buildings Made of Reinforced Concrete with Cavity Walls. *Heliyon* **2024**, *10*, e30653. [CrossRef]
11. Channels, H. Analysis of Thermal Resistance of Developed Energy-Saving. *Buildings* **2023**, *13*, 356. [CrossRef]
12. Naje, W.A.; Hasan, Z.M.; Al-Fahham, M.A. Simulation by Using ANSYS—FLUENT of Wall Room with Effect Air Gaps Between Walls. *Int. J. Intell. Syst. Appl. Eng.* **2023**, *11*, 78–84.
13. Kaynakli, O. Parametric Investigation of Optimum Thermal Insulation Thickness for External Walls. *Energies* **2011**, *4*, 913–927. [CrossRef]
14. Sadrzadehrafiei, S.; Sopian, K.; Mat, S.; Lim, C.; Hashim, H.S.; Zaharim, A. Potential Energy and Emission Reduction through Application of Triple Glazing. In *Recent Researches in Environment and Biomedicine*; University Kebangsaan Malaysia: Bangi, Malaysia, 2012; ISBN 978-1-61804-075-6.
15. Liao, W.; Wen, C.; Luo, Y.; Peng, J.; Li, N. Influence of Different Building Transparent Envelopes on Energy Consumption and Thermal Environment of Radiant Ceiling Heating and Cooling Systems. *Energy Build.* **2022**, *255*, 111702. [CrossRef]
16. Influence of Glazed Façades on Energy Consumption for Air Conditioning of Office Buildings in Brazilian Climates. Available online: https://www.researchgate.net/publication/313697169_Influence_of_Glazed_Facades_on_Energy_Consumption_for_Air_Conditioning_of_Office_Buildings_in_Brazilian_Climates (accessed on 21 August 2024).
17. Hamza, N. Double versus Single Skin Facades in Hot Arid Areas. *Energy Build.* **2008**, *40*, 240–248. [CrossRef]
18. Baetens, R.; Jelle, B.P.; Gustavsen, A. Properties, Requirements and Possibilities of Smart Windows for Dynamic Daylight and Solar Energy Control in Buildings: A State-of-the-Art Review. *Sol. Energy Mater. Sol. Cells* **2010**, *94*, 87–105. [CrossRef]
19. Islam, H.; Zhang, G.; Setunge, S.; Bhuiyan, M.A. Life Cycle Assessment of Shipping Container Home: A Sustainable Construction. *Energy Build.* **2016**, *128*, 673–685. [CrossRef]
20. Kon, O.; Caner, İ. Life Cycle Cost Analysis of the Buildings in Turkey Related to Energy Consumption Due to External Wall Insulation. In *Green Energy and Technology*; Springer: Cham, Switzerland, 2020; pp. 123–135. [CrossRef]
21. Dlimi, M.; Iken, O.; Agounoun, R.; Zoubir, A.; Kadiri, I.; Sbai, K. Energy Performance and Thickness Optimization of Hemp Wool Insulation and Air Cavity Layers Integrated in Moroccan Building Walls. *Sustain. Prod. Consum.* **2019**, *20*, 273–288. [CrossRef]
22. Altin, M.; Yildirim, G.Ş. Investigation of Usability of Boron Doped Sheep Wool as Insulation Material and Comparison with Existing Insulation Materials. *Constr. Build. Mater.* **2022**, *331*, 127303. [CrossRef]
23. Ali, M.H.; Mawlood, M.K.; Jalal, R.E. Investigating the Impact of Trombe Wall Parameters on Thermal Performance and Room Temperature in the Iraqi Climate. *Heat Transf.* **2024**, *53*, 2600–2635. [CrossRef]
24. Fantozzi, F.; Galbiati, P.; Leccese, F.; Salvadori, G.; Rocca, M. Thermal Analysis of the Building Envelope of Lightweight Temporary Housing. *J. Phys. Conf. Ser.* **2014**, *547*, 012011. [CrossRef]
25. Plastering | Plaster Volume Calculator | Calculation of Materials for Plastering. Available online: https://civil-engineering-calculators.com/Quantity-Estimator/Plastering-Calculator#google_vignette (accessed on 22 August 2024).
26. Polyethylene Terephthalate (PET) Prices, Monitor & Demand. Available online: https://www.chemanalyst.com/Pricing-data/polyethylene-terephthalate-72 (accessed on 22 August 2024).
27. Argon—United States—2007–2023—Market Overview—IndexBox Platform. Available online: https://app.indexbox.io/report/080410/0/ (accessed on 22 August 2024).
28. Bergman, T.L.; Lavine, A.S.; Incropera, F.P.; DeWitt, D.P. *Fundamentals of Heat and Mass Transfer*, 8th ed.; Wiley: Hoboken, NJ, USA.
29. Moukalled, F.; Mangani, L.; Darwish, M. The Finite Volume Method. In *The Finite Volume Method in Computational Fluid Dynamics. Fluid Mechanics and Its Applications*; Springer: Cham, Switzerland; Volume 113.
30. Hirpho, M. Mixed Convection of Casson Fluid in a Differentially Heated Bottom Wavy Wall. *Heliyon* **2021**, *7*, e07361. [CrossRef] [PubMed]
31. ANSYS, Inc. *ANSYS Fluent documentation: User guide,(n.d.)*; ANSYS, Inc.: Canonsburg, PA, USA, 2016.
32. Omle, I.; Kovács, E.; Bolló, B. Applying Recent Efficient Numerical Methods for Long-Term Simulations of Heat Transfer in Walls to Optimize Thermal Insulation. *Results Eng.* **2023**, *20*, 101476. [CrossRef]
33. Kadhim, S.A.; Ibrahim, O.A.A.-M. The Effect of Holes Number in Cylindrical Samples on the Forced Convection Heat Flow. *Int. J. Mech. Eng. Robot. Res.* **2022**, *11*, 429–436. [CrossRef]
34. Wang, H.; Xin, S.; Le Quéré, P. Étude Numérique Du Couplage de La Convection Naturelle Avec Le Rayonnement de Surfaces En Cavité Carrée Remplie d'air. *Comptes Rendus-Mec.* **2006**, *334*, 48–57. [CrossRef]
35. Laaroussi, N. Contribution à La Simulation Numérique Des Transferts de Chaleur Par Conduction, Rayonnement et Convection Thermosolutale Dans Des Cavités. Ph.D. Thesis, Université Paris-Est, Paris, France, 2008.
36. Omle, I.; Askar, A.H.; Kovács, E.; Bolló, B. Comparison of the Performance of New and Traditional Numerical Methods for Long-Term Simulations of Heat Transfer in Walls with Thermal Bridges. *Energies* **2023**, *16*, 4604. [CrossRef]
37. Mathews, P.G. *Design of Experiments with MINITAB*; Quality Press: Mumbai, India, 2004.
38. Zhang, X.; Xie, Y.; Han, J.; Wang, Y. Design of Control Valve with Low Energy Consumption Based on Isight Platform. *Energy* **2022**, *239*, 122328. [CrossRef]
39. Isight Simulia-Isight-Brochure.Pdf (3ds.Com. Available online: https://www.3ds.com/fileadmin/PRODUCTS-SERVICES/SIMULIA/RESOURCES/DS_SIMULIA_IsightV40_GettingStartedGuide.pdf (accessed on 8 December 2024).

40. Nyers, A.; Nyers, J. Enhancing the Energy Efficiency—COP of the Heat Pump Heating System by Energy Optimization and a Case Study. *Energies* **2023**, *16*, 2981. [CrossRef]
41. Askar, A.H.; Kovács, E.; Bolló, B. Prediction and Optimization of Thermal Loads in Buildings with Different Shapes by Neural Networks and Recent Finite Difference Methods. *Buildings* **2023**, *13*, 2862. [CrossRef]
42. Duffie, J.A.; Beckman, W.A. Selected Heat Transfer Topics. In *Solar Engineering of Thermal Processes*, 4th ed.; John Wiley & Sons Inc.: Hoboken, NJ, USA, 2013; pp. 138–172.
43. 2005 Ashrae Handbook Fundamentals. I-P Edition. Supported by ASHRAE Research | PDF | Air Conditioning | Ventilation (Architecture). Available online: https://www.scribd.com/document/604053106/2005-ASHRAE-HANDBOOK-FUNDAMENTALS-I-P-Edition-Supported-by-ASHRAE-Research (accessed on 8 December 2024).
44. Kadhim, S.A.; Al-Ghezi, M.K.S.; Shehab, W.Y. Optimum Orientation of Non-Tracking Solar Applications in Baghdad City. *Int. J. Heat Technol.* **2023**, *41*, 125–134. [CrossRef]
45. Singh, A.; Mourelatos, Z.P.; Li, J. Design for Lifecycle Cost Using Time-Dependent Reliability. *J. Mech. Des.* **2010**, *132*, 9. [CrossRef]